

# Practical Uncertainty Minimization for Spectral Macrostate Data Clustering

Brian White\* and David Shalloway†

Biophysics Program, Department of Molecular Biology and Genetics, Cornell University, Ithaca, New York 14853

Spectral clustering, which uses the global information embedded in eigenvectors of an inter-item relation matrix, can outperform traditional approaches such as  $k$ -means and hierarchical clustering. Spectral hierarchical bipartitioning is well-understood, but spectral multipartitioning remains an interesting research topic. Korenblum and Shalloway [Phys. Rev. E **67**, 056704 (2003)] used an analogy to the dynamic coarse-graining of a stochastic system and the principle of cluster uncertainty minimization to motivate a fuzzy spectral multipartitioning method, macrostate data clustering (MDC), that could solve problems that defeated other methods. However, MDC poses a challenging non-convex global optimization problem that was solved by a brute-force technique unlikely to scale to problem sizes beyond  $O(10^2)$ . Here we provide further tests of the accuracy of MDC and develop a new method for solving the optimization problem, which scales to data sets at least two orders-of-magnitude larger. This range includes problems of significant biological interest, such as microarray analysis of gene expression data. Moreover, we show that the method of Weber et al. [Tech. Rep. 04-39, Konrad-Zuse-Zentrum für Informationstechnik Berlin (2004)] provides a zeroth-order solution to the minimum uncertainty problem and provide a new geometric interpretation of the solution. We show how this approximation can be naturally extended to an exact solution and how the conditions for its validity can be extended past those previously proposed.

## I. INTRODUCTION

Coarse-graining data *items*  $i$  ( $1 \leq i \leq N$ ) into *clusters*  $\alpha$  ( $1 \leq \alpha \leq m$ ) is important for large-scale data analysis. For example, clustering genes according to their microarray expression profiles allows biologists to subsequently infer potential *cis*-regulatory elements from sequence commonalities within the clusters [1]. A clustering solution defines *assignment vectors*  $\mathbf{w}_\alpha \equiv [w_\alpha(1), w_\alpha(2), \dots, w_\alpha(N)]$ , where  $w_\alpha(i)$  is the “grade of membership” of item  $i$  with respect to cluster  $\alpha$ . This may be made more precise by insisting on a *fuzzy clustering* solution that satisfies the probabilistic constraints

$$w_\alpha(i) \geq 0 \quad (\forall \alpha, i) \quad (1a)$$

$$\sum_{\alpha} w_\alpha(i) = 1 \quad (\forall i) \quad (1b)$$

and thus defines  $w_\alpha(i)$  as the probability that item  $i$  is a member of cluster  $\alpha$ . This can be useful in data modeling: For example, the probabilistic assignments of individuals to populations (i.e., clusters) based on genotypic data may indicate the presence of an admixed individual, whose genetic makeup is consistent with several populations, or a migrant, whose relatively weak population assignment may suggest immigration into that population in the distant past [2, 3]. In some cases it is adequate to ignore uncertainty and simply partition the items via a *hard clustering* that enforces  $w_\alpha(i) \in \{0, 1\}$ . This can be done by quantizing a fuzzy clustering (i.e., assigning item  $i$  completely to the cluster having the largest assignment

value). Some methods (e.g., *k-means*) only provide hard clusterings, so no probabilistic information is available.

Clustering typically proceeds from an  $N \times N$  *similarity matrix*  $S$ , where the off-diagonal element  $S_{ij}$  provides an inverse indicator of the “distance” between items  $i$  and  $j$ . The primary data may directly define the  $S_{ij}$  (e.g., the alignment scores from sequence comparisons or edge weights of a graph). Alternatively, the data may consist of  $N_D$  *properties* for each item that can be embedded in a metric space. In that case, the data are consolidated into an  $N \times N_D$  matrix  $X$ , where  $X_{ia}$  is the  $a^{\text{th}}$  property of item  $i$ . For example, in microarray analysis each gene is an item and its properties are its  $N_D$  expression levels under  $N_D$  different conditions. Distances  $d_{ij}$  may be defined via a problem-specific Euclidean metric tensor  $g$ :

$$d_{ij} = \left[ \sum_{a,b=1}^{N_D} (X_{ia} - X_{ja}) g_{ab} (X_{ib} - X_{jb}) \right]^{1/2}. \quad (2)$$

$g$  is the identity when the properties are independent and need no pre-conditioning (i.e., have equal importance), but may otherwise be adjusted to account for correlations and/or data scale anisotropies.  $S$  is then defined by  $S_{ij} = f(d_{ij})$ , where  $S_{ij} \geq 0$  and  $f$  is often an exponentially decaying function.

Traditional partitioning methods impose characteristic shapes on the clusters. For example,  $k$ -means and complete-linkage clustering generate convex clusters while single-linkage clustering generates unbalanced and straggly clusters [4]. These shapes may not reflect the true geometries of the problem (e.g., the irregular boundaries of an object within an image [5]). However, arbitrary cluster shapes can be generated by *spectral clustering*, and they have outperformed  $k$ -means across several synthetic benchmarks [6, 7, 8]. They accomplish this by

\*Electronic address: bsw27@cornell.edu

†Electronic address: dis2@cornell.edu

analyzing the eigensystem of a *transition* (or *Laplacian*<sup>1</sup>) matrix  $\Gamma$ :

$$\Gamma = D_S - S, \quad (3)$$

where  $D_S$  is the diagonal matrix of column sums of  $S$ :  $D_{Sjj} = \sum_i S_{ij}$ . Hence,

$$\Gamma_{ij} \leq 0 \quad (\forall i \neq j) \quad (4a)$$

$$\mathbf{1} \cdot \Gamma = 0, \quad (4b)$$

where  $\mathbf{1}$  is the item-space vector having all components equal to unity and  $\cdot$  denotes the item-space inner product:  $\mathbf{x} \cdot \mathbf{y} \equiv N^{-1} \sum_{i=1}^N x_i y_i$ . These equations imply that the eigenvalues  $\gamma_n$  and left eigenvectors  $\psi_n$  of  $\Gamma$  satisfy<sup>2</sup>

$$\gamma_0 = 0; \gamma_{n>0} \geq 0 \quad (5a)$$

$$\psi_0 = \mathbf{1}. \quad (5b)$$

Spectral clustering methods embed each item  $i$  into the linear space  $\mathbb{R}^N$  using the vector components  $\psi_0(i), \psi_1(i), \dots, \psi_{N-1}(i)$  as coordinates. Because the low-frequency eigenvectors have longer “wavelengths,” they provide a natural basis for coarse-graining. Therefore, it is sensible to project into the *low-frequency* (or *clustering*) *subspace* wherein items are represented by the low-frequency *clustering eigenvectors*  $\vec{\psi}(i) \equiv [\psi_0(i), \psi_1(i) \dots \psi_{m-1}(i)]$ , where  $m$  is the number of clusters.<sup>3</sup> While some methods fix  $m$  *a priori*, others use a *spectral gap* condition:

$$0 = \gamma_0 < \gamma_1 < \dots \gamma_{m-1} \ll \gamma_m. \quad (6)$$

The presence of such a gap suggests the existence of a corresponding gap in the spatial fluctuation scale (owing to the inverse relationship between frequency and wavelength) that naturally sets a scale for clustering.

Methods differ in how they use the  $\vec{\psi}(i)$  to define a clustering. *Spectral bipartitioning* approaches (Ref. 10, for history and review) fix  $m = 2$ . They order the items according to  $\psi_1(i)$  (since  $\psi_0$  is a constant, it provides no information) and then partition them into hard clusters by choosing a separation point (e.g., according to the sign of  $\psi_1(i)$  or its position relative to the median). These approaches can be extended to  $m = 2^k$  clusters by recursion [11], typically after fixing  $k$  *a priori*.

Unfortunately, hierarchical bipartitioning sometimes fails to respect natural cluster boundaries, and better results can be obtained using non-hierarchical  $m$ -way spectral clustering approaches [12, 13, 14]. One way to do

this has been to partition the items based on their low-frequency subspace coordinates using  $k$ -means [7, 15, 16] or *normalized-cut* objective function minimization [17]. The induced partitionings are necessarily hard.

Korenblum and Shalloway [8] developed a fuzzy  $m$ -way spectral clustering method using a different approach: They likened clustering to coarse-graining of a dynamic classical stochastic system [18]. In this picture, each cluster is viewed as a metastable macroscopic state of a diffusive relaxation process governed by  $\Gamma$ , which now acts as a dynamical transition matrix. Their *macrostate data clustering* (MDC) approach defines the  $\mathbf{w}_\alpha$  as linear combinations of the  $m$  clustering eigenvectors,

$$\mathbf{w}_\alpha = \sum_{n=0}^{m-1} M_{\alpha n} \psi_n \equiv \vec{M}_\alpha \circ \vec{\psi}, \quad (7)$$

where the  $\vec{M}_\alpha \equiv [M_{\alpha 0}, M_{\alpha 1}, \dots, M_{\alpha(m-1)}]$  are  $m$ -vectors,  $\vec{\psi} \equiv [\psi_0, \psi_1, \dots, \psi_{m-1}]$ , and  $\circ$  denotes the inner product over the low-frequency subspace, i.e.,

$$\vec{x} \circ \vec{y} = \sum_{n=0}^{m-1} x_n y_n.$$

Eqs. (1) and the independence of the  $\psi_n$  imply constraints on the  $\vec{M}_\alpha$ :

$$\mathbf{w}_\alpha(i) = \vec{M}_\alpha \circ \vec{\psi}(i) \geq 0 \quad (\forall \alpha, i) \quad (8a)$$

$$\sum_\alpha \vec{M}_\alpha = \hat{\epsilon}_0, \quad (8b)$$

where  $\hat{\epsilon}_0$  is the  $m$ -vector  $(1, 0, \dots, 0)$ .

Eq. (7) transforms the clustering problem to that of determining the optimal  $\vec{M}_\alpha$  subject to Eqs. (8). Since the  $\mathbf{w}_\alpha$  are non-negative and composed of only the long-wavelength  $\psi_{n < m}$  they will, in general, overlap each other,

$$\mathbf{w}_\alpha \cdot \mathbf{w}_\beta \geq 0, \quad (9)$$

and the item-to-cluster assignments will inherently be uncertain, i.e., fuzzy. In MDC the “best” clustering is defined as that having *minimum uncertainty*, so the optimal  $\vec{M}_\alpha$ , and hence optimal clustering, is determined by minimizing an uncertainty-measuring objective function subject to the constraints of Eq. (1). Acceptable clusterings are determined by the spectral gap condition of Eq. (6) and a minimum certainty parameter.

However, uncertainty minimization presents a challenging constrained, non-convex optimization problem. While Korenblum and Shalloway demonstrated the ability of MDC to solve difficult problems, they did so using a “brute-force” solver whose  $O(m^2 N^{m+1})$  computational complexity limited its application to modest-sized problems ( $N = 200$ ) and precluded application to the larger problems [e.g.,  $N \sim O(10^4)$ ] that emerge in areas such as gene microarray analysis [19].

<sup>1</sup> Spectral graph theory methods sometimes analyze the *normalized Laplacian*  $\mathcal{L} \equiv D_S^{-\frac{1}{2}} \Gamma D_S^{-\frac{1}{2}}$ . Related methods analyze the Markov matrix  $T \equiv D_S^{-\frac{1}{2}} S D_S^{-\frac{1}{2}} = I - \mathcal{L}$ , where  $I$  is the identity matrix.

<sup>2</sup>  $\psi_0$  may be chosen to satisfy Eq. (5b) even in a degenerate system having multiple zero eigenvalues.

<sup>3</sup> An exception is Ref. 9, which uses more eigenvectors in the projected representation than  $m$ .

Subsequently, Weber et al. [20] introduced a more efficient approximate fuzzy clustering method that was motivated by perturbative analysis of almost-block diagonal matrices [21]. Their Perron cluster analysis (PCCA) also uses Eq. (7) but with the  $\mathbf{w}_\alpha$  defined as “membership functions” that only approximate the probabilistic non-negativity constraints of Eq. (1a). In PCCA the  $\vec{M}_\alpha$  are determined algorithmically, not by objective function optimization, and clusterings for different values of  $m$  are accepted if the resultant approximation is regarded by somewhat subjective criteria to be adequate. While approximate, this method had the advantage of being computationally simpler than MDC.

In this paper we show that the MDC uncertainty minimization problem has geometric interpretations that can be exploited to obtain a zeroth-order solution to the global problem, which can then be locally refined towards an exact solution using standard linear programming methods. The algorithm is computationally efficient and allows MDC to solve an  $m = 10, N = 20,000$  problem in about one minute on a commodity processor. Secondly, we show that the PCCA membership functions can be viewed as approximate solutions to the minimum uncertainty condition, thus establishing a connection between uncertainty minimization and block-diagonal matrix perturbation. Using this connection, we extend the previously reported conditions under which the PCCA approximation is applicable.

## II. REVIEW OF MDC

Shalloway [18] has described how spectral analysis of continuous stochastic dynamics can be used to fuzzily dissect configuration space into macroscopic regions (*macrostates*), which provide a coarse-grained representation for describing metastable dynamic relaxations. Korenblum and Shalloway [8] adapted this approach to data clustering by modeling the set of items as a discrete diffusive system and regarding  $\Gamma_{ij}$  as the stochastic transition rate between items  $i$  and  $j$ . Using dimensional analysis and considering occlusion of diffusive flow by intervening items, they suggested<sup>4</sup>

$$\Gamma_{ij} = -\frac{e^{-(d_{ij})^2/2\langle d_0^2 \rangle}}{(d_{ij})^2} \quad (i \neq j) \quad (10a)$$

$$\Gamma_{ii} = -\sum_{j \neq i} \Gamma_{ji} \quad (10b)$$

$$\langle d_0^2 \rangle = N^{-1} \sum_{i=1}^N (d_{i<})^2, \quad (10c)$$

where  $d_{i<} \equiv \min_{j \neq i} d_{ij}$ .

Defining the time-dependent ensemble probability vector  $\mathbf{p}(t)$ , where  $p_i(t)$  is the probability of occupation of item  $i$  at time  $t$ , they then introduced diffusive dynamics using the master equation

$$\frac{d\mathbf{p}(t)}{dt} = -\Gamma \cdot \mathbf{p}(t). \quad (11)$$

$\Gamma$  has non-negative eigenvalues [8] and its left and right eigenvectors are equal and orthogonal and may be normalized so that

$$\psi_m \cdot \psi_n = \delta_{mn}.$$

Eq. (11) has the solution

$$\mathbf{p}(t) = \sum_{n=0}^{\infty} c_n e^{-\gamma_n t} \psi_n, \quad (12)$$

which describes relaxation to equilibrium. It can be shown that Eqs. (4) and (11) ensure that all components of  $\mathbf{p}(t)$  remain non-negative during this relaxation.

This and related [15, 22, 23, 24, 25] dynamical metaphor provides *ex post facto* justification for common practices within the spectral clustering community, including the form of  $\Gamma$ , the use of low-frequency subspaces, and the requirement for a spectral gap. For example, early approaches [7, 26] analyzed, without explanation, a  $\Gamma$  matrix having an exponential numerator as in Eq. (10a). Moreover, Eq. (4b) [equivalently, (10b)] is now interpreted as dynamical conservation of probability. Furthermore, since the eigenvalues now describe transition rates, the spectral gap of Eq. (6) indicates that dynamics can be separated into fast modes  $\psi_{n \geq m}$  that redistribute probability *within*  $m$  weakly-communicating subregions (or clusters) and slow modes  $\psi_{n < m}$  that redistribute probability *between* clusters.

MDC determines  $m$  by the spectral gap condition and then determines the optimal  $\vec{M}_\alpha$  by minimizing the cluster overlap uncertainties expressed by Eqs. (9). As discussed in Ref. 8, minimizing these is equivalent to maximizing the  $\mathbf{w}_\alpha \cdot \mathbf{w}_\alpha$ . Normalizing for cluster size, MDC maximizes the geometric mean of the *fractional cluster certainties*  $\bar{\Upsilon}_\alpha(M)$  ( $1 \leq \alpha \leq m$ ),

$$\bar{\Upsilon}_\alpha(M) \equiv \frac{\mathbf{w}_\alpha \cdot \mathbf{w}_\alpha}{\mathbf{1} \cdot \mathbf{w}_\alpha}, \quad (13)$$

where  $M$  represents the components of all the  $\vec{M}_\alpha$ . The *overall uncertainty function*  $\Phi(M)$ ,

$$\Phi(M) \equiv -\sum_{\alpha} \log \bar{\Upsilon}_\alpha(M), \quad (14)$$

provides the global minimization objective function that determines  $M$ . The clustering specified by this solution is accepted only if

1. The spectral gap condition Eq. (6) is satisfied for a *minimum gap parameter*  $\rho_\gamma$

$$\gamma_m / \gamma_{m-1} > \rho_\gamma. \quad (15)$$

<sup>4</sup> Without loss of generality, the diffusion coefficient, which would normally appear in Eq. (10a), is set to unity.

2. The  $w_\alpha$  are not excessively fuzzy. Quantitatively, we require that

$$\overline{\Upsilon}_\alpha(M) > \rho_\Upsilon \quad (\forall \alpha), \quad (16)$$

where  $\rho_\Upsilon$  is the *minimum certainty parameter*.

Because  $\Phi(M)$  is invariant under permutations of the indexes associated with the clusters, its global minimum will have a  $m!$ -fold permutation degeneracy.

### III. COMPUTATIONAL THEORY

Minimization of  $\Phi(M)$  subject to the constraints of Eq. (8) poses a global, non-linear optimization problem with respect to the  $m^2$  degrees-of-freedom of  $M$ . We first describe two geometric representations of the problem in Sec. III A that illuminate the problem and then show how to solve it in three steps: (1) precondition  $\Gamma$  to avoid numerical noise that can obfuscate spectral gaps when low-lying eigenvalues are nearly degenerate, to improve numerical efficiency, and to remove outliers (Appendix A), (2) find a zeroth-order solution (Sec. III B), and (3) determine the exact solution by iterative refinement using linear programming with a subset of the inequality constraints (Sec. III C).

#### A. Geometric representation of uncertainty minimization

##### 1. Symmetric $M$ -representation

Each  $\vec{M}_\alpha$  may be regarded as the coordinates of a particle  $\alpha$  in  $\mathbb{R}^m$  with axes labeled  $M_0, M_1, \dots, M_{(m-1)}$ . Eq. (8a) implies that the same  $N$  inequality constraints act on each particle: The inequality constraint associated with item  $i$  is identical for each  $\alpha$  and thus restricts each  $\vec{M}_\alpha$  to the same feasible half-space in  $\mathbb{R}^m$ . This is bounded by a hypersurface that passes through the origin and is normal to  $\vec{\psi}(i)$ . The intersection of these half-spaces determines the feasible region as a convex polyhedral cone in the upper half of  $\mathbb{R}^m$ . Only a subset of the inequality constraints will actually bound the feasible region, since their satisfaction will automatically guarantee satisfaction of the other constraints. And, as proved in Appendix B 1, each particle lies on an edge of the polyhedral cone (i.e., is constrained by  $m-1$  *active* inequality constraints) at every local minimizer of  $\Phi(M)$ .

An example of this *symmetric  $M$ -representation* for  $m=2$  is shown in Fig. 1(a). In this case, the feasible region is bounded by only two lines corresponding to  $\vec{M} \circ \vec{\psi}(i_<) = 0$  and  $\vec{M} \circ \vec{\psi}(i_>) = 0$ , where  $i_<$  and  $i_>$  are the minimizer and maximizer of  $\psi_1(i)$ , respectively. The global minimum of  $\Phi$  corresponds to the unique (up to the permutation degeneracy) situation where each particle lies on the feasible region boundary while the equality

constraints of Eq. (8b) are simultaneously satisfied. In the example shown in the figure, this is when the points lie within the two squares on the boundary. The two ways of associating the particles with the squares corresponds to the 2-fold permutation degeneracy of the solution.

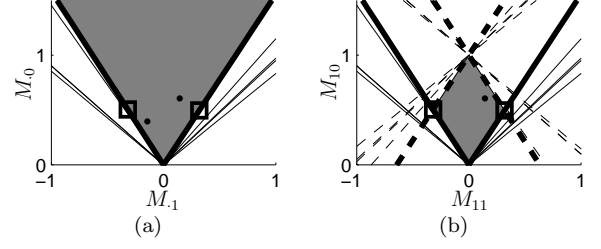


FIG. 1: Symmetric and asymmetric  $M$ -representations of a  $m=2$  problem. (a) *Symmetric  $M$ -representation*: The diagonal lines indicate the boundaries of the inequality constraints. The two bold lines forming the narrowest cone (shaded) define the feasible region in  $\mathbb{R}^m = \mathbb{R}^2$ .  $\vec{M}_1$  and  $\vec{M}_2$  are represented by dots. They are not independent since they are further constrained by the equality constraints Eq. (8b). The global minimum of the uncertainty objective function  $\Phi(M)$  corresponds to the dots being located at the positions indicated by small squares, and the invariance under particle exchange corresponds to the permutation degeneracy discussed in the text. (b) *Asymmetric  $M$ -representation*: The solid lines indicate the boundaries of the homogeneous inequality constraints acting on the free particle  $\vec{M}^{\text{free}} = \vec{M}_1$ . The dashed lines indicate the boundaries of the inhomogeneous inequality constraints that derive from the slave particle  $\vec{M}_2$ . Two of these (bold-dashed) lines cap the cone formed by the relevant homogeneous constraint boundaries (bold) to define a closed feasible polytope in  $\mathbb{R}^{m(m-1)} = \mathbb{R}^2$ . In this representation the single dot represents all  $m(m-1) = 2$  components of  $\vec{M}^{\text{free}}$ .  $\Phi(M)$  is minimized at either of the two permutation-degenerate solutions (small squares).

##### 2. Asymmetric $M$ -representation

The  $m$  particles in the symmetric  $M$ -representation are not independent because of the equality constraints [Eq. (8b)]. We use these in the *asymmetric  $M$ -representation* to explicitly eliminate the degrees-of-freedom of one *slave* particle that, without loss of generality, we take to be  $\vec{M}_m$ :

$$\vec{M}_m = \hat{\varepsilon}_0 - \sum_{\alpha \neq m} \vec{M}_\alpha. \quad (17)$$

The homogeneous inequality constraints on the slave,  $\vec{M}_m \circ \vec{\psi}(i) \geq 0$  ( $\forall i$ ), transform into inhomogeneous inequality constraints that couple the remaining  $m-1$  *free* particles:

$$\sum_{\alpha \neq m} \vec{M}_\alpha \circ \vec{\psi}(i) \leq 1. \quad (18)$$



We consolidate the  $m(m-1)$  degrees of freedom of the free particles into the supervector  $\vec{M}^{\text{free}}$  having components  $(\vec{M}_1, \vec{M}_2, \dots, \vec{M}_{m-1})$  in  $\mathbb{R}^{m(m-1)}$ . Optimization then proceeds in  $\mathbb{R}^{m(m-1)}$  with the  $\vec{M}^{\text{free}}$  restricted by  $(m-1) \times N$  homogeneous inequality constraints from Eq. (8a) with  $1 \leq \alpha < m$  and  $N$  inhomogeneous inequality constraints from Eq. (18). The combination of homogeneous and inhomogeneous inequality constraints forms a closed convex polytope that bounds the feasible region. Each local minimum of  $\Phi(M)$  (and thus, the global minimum) lies at a vertex of this polytope [8].

An example of the asymmetric  $M$ -representation for  $m = 2$  is shown in Fig. 1(b). In this case there are four bounding constraints: two homogeneous inequality constraints having boundaries passing through the origin and two inhomogeneous inequality constraints (from the slave cluster) with boundaries intersecting at  $\hat{\varepsilon}_0$ .<sup>5</sup>  $\Phi$  is infinite at the polytope vertices at the origin and  $\hat{\varepsilon}_0$ . The two other vertices correspond to index-permutation-equivalent global minima.

The minimization problem can be visualized and easily solved in this manner only for  $m = 2$ : As  $m$  increases the number of polytope vertices, and hence the number of local minima, grows rapidly and the global minimization problem becomes difficult. Korenblum and Shalloway [8] used a brute-force method that randomly explored different vertices. However, this method was inefficient and limited MDC to problems of size  $N = O(10^2)$ .

## B. Representatives and the approximate global solution

We take a different approach: Rather than trying to identify the global minimizing vertex directly, we exploit the fact that the  $m^2$  components of  $M$  can be determined by the  $m^2$  low-frequency components of an appropriately chosen subset  $\mathcal{R} = \{r_1, r_2, \dots, r_m\}$  of  $m$  items, which we call *representatives*. To make this explicit we write a matrix analog of Eq. (7) over  $\mathcal{R}$  as

$$W^{\mathcal{R}} = M \circ \Psi^{\mathcal{R}}, \quad (19)$$

<sup>5</sup> For  $m > 2$ , the slave inequality constraint boundaries do not intersect at a point but in the subspace where Eq. (18) is an equality for all items. This condition can be expressed as  $\sum_{k=1}^{m(m-1)} Z_{ik} M_k^{\text{free}} = 1$  ( $\forall i$ ), where  $M_k^{\text{free}} \equiv M_{\alpha,n}$  with  $\alpha \equiv 1 + \left\lfloor \frac{k-1}{m} \right\rfloor$ ,  $n \equiv (k-1) \bmod m$ , and  $Z_{ik} \equiv \psi_{k'}(i)$  with  $k' \equiv (k-1) \bmod m$ . ( $M_k^{\text{free}}$  is the flattened form of the supervector  $\vec{M}^{\text{free}}$ .)  $Z_{ik}$  has  $m$  independent columns, i.e., it contains  $m-1$  copies of each of the  $m$  low-frequency  $\psi_n$ . Therefore, its rank is  $m$  and it only imposes  $m$  restrictions on the  $m(m-1)$  variables. Thus, the intersection of the inhomogeneous constraints occurs in a subspace of dimension  $m(m-1) - m = m(m-2)$ .

where

$$W_{\alpha\beta}^{\mathcal{R}} = w_{\alpha}(r_{\beta}) \quad (1 \leq \alpha, \beta \leq m) \quad (20a)$$

$$\Psi_{n\alpha}^{\mathcal{R}} = \psi_n(r_k) \quad \begin{cases} (1 \leq \alpha \leq m) \\ (0 \leq n < m) \end{cases} \quad (20b)$$

and  $M$  is the matrix having the  $\vec{M}_{\alpha}$  as its rows. According to Eq. (8b),  $M$  must satisfy

$$\sum_{\alpha} M_{\alpha n} = \delta_{n0}. \quad (21)$$

As shown in Appendix B 2, there always exists at least one subset  $\mathcal{R}$  such that  $\Psi^{\mathcal{R}}$  is invertible. With such a subset we can solve Eq. (19) for  $M$ :

$$M = W^{\mathcal{R}} \bullet (\Psi^{\mathcal{R}})^{-1}, \quad (22)$$

where  $\bullet$  denotes the inner product over the cluster index  $\alpha$ .

The usefulness of Eq. (22) may be questioned since we do not know any  $W^{\mathcal{R}}$  exactly *a priori*. However, any data set amenable to clustering will have at least one item per cluster that will be strongly assigned in the clustering solution; we call such items *candidate representatives*. If we could select a set of representatives  $\mathcal{R}_c$  containing one candidate representative from each cluster, we could use our approximate foreknowledge of their assignment values to approximate  $W^{*\mathcal{R}_c}$ ,  $W^{\mathcal{R}_c}$  at the solution. Then, via Eq. (22), we could approximate  $M^*$ , the solution.

For example, if item  $i_{\alpha}$  were a candidate representative for cluster  $\alpha$  then its assignment in the clustering solution would be<sup>6</sup>

$$w_{\beta}^*(i_{\alpha}) \approx \delta_{\alpha\beta}. \quad (23)$$

By choosing  $r_{\alpha} = i_{\alpha}$  for cluster  $\alpha$  and making similar choices for the other clusters we would get

$$W^{*\mathcal{R}_c} \approx I. \quad (24)$$

This zeroth-order estimate could be used to approximately solve Eq. (22) for  $M^*$ :

$$M^* = W^{*\mathcal{R}_c} \cdot (\Psi^{\mathcal{R}_c})^{-1} \quad (25a)$$

$$\approx I \cdot (\Psi^{\mathcal{R}_c})^{-1} = (\Psi^{\mathcal{R}_c})^{-1} \equiv M^0. \quad (25b)$$

In agreement with Eq. (21),  $M^0$  would satisfy<sup>7</sup>

$$\sum_{\alpha} M_{\alpha n}^0 = \delta_{n0}. \quad (26)$$

<sup>6</sup> Eq. (23) breaks the permutation symmetry by assigning each representative to a specific cluster index.

<sup>7</sup> To prove this, note that Eq. (19) with  $W^{\mathcal{R}} \rightarrow I$  implies that  $1 = \sum_{\alpha} I_{\alpha\beta} = \sum_{\alpha} W_{\alpha\beta}^{\mathcal{R}_c} = \sum_{\alpha n} M_{\alpha n}^0 \Psi_{n\beta}^{\mathcal{R}_c}$  ( $\forall \beta$ ). Since  $\Psi_{0\beta}^{\mathcal{R}_c} = \psi_0(r_{\beta}) = 1$  ( $\forall \beta$ ), this is solved by  $\sum_{\alpha} M_{\alpha n}^0 = \delta_{n0}$ . Moreover, since  $\Psi^{\mathcal{R}}$  is invertible, this solution is unique, thereby proving Eq. (26).

Knowing  $M^0$  would allow us to define zeroth-order estimates  $\mathbf{w}_\alpha^0$  for *all* the items via Eq. (7) with  $\vec{M}_\alpha \rightarrow \vec{M}_\alpha^0$ , where the  $\vec{M}_\alpha^0$  are the rows of  $M^0$ :

$$\mathbf{w}_\alpha^0 = \vec{M}_\alpha^0 \circ \vec{\psi}. \quad (27)$$

However, the  $\mathbf{w}_\alpha^0$  would not necessarily satisfy the inequality constraints of Eq. (1a). If they did, they would solve the optimization problem. If they didn't, they would provide a starting point for refining the solution as discussed in Sec. III C.

### 1. Finding $\mathcal{R}_c$

Eq. (25b) implies that we only need to find the representatives to determine  $M^0$ . This is trivial when  $m = 2$ : The two active inequality constraints [identified by the bold and bold-dashed lines in Fig. 1(b)] come from items  $r_1$  and  $r_2$ , corresponding to  $\psi_1(r_1) = \max_i \psi_1(i)$  and  $\psi_1(r_2) = \min_i \psi_1(i)$ . Thus, at the solution  $w_1^*(r_2) = 0$  and  $w_2^*(r_1) = 0$ , and the equality constraints imply that  $w_1^*(r_1) = 1$  and  $w_2^*(r_2) = 1$ . Thus,  $r_1$  and  $r_2$  not only generate the active constraints, but are also the representatives, which in this case are perfectly assigned in the solution.

The situation is more complicated when  $m > 2$ . The representatives: (1) may not be maxima and minima of the eigenvectors, (2) may not be the items associated with the active constraints, and (3) may not be perfectly assigned at the solution. Nonetheless, as discussed above, they will satisfy  $w_\alpha(r_\beta) \approx \delta_{\alpha\beta}$ , even for  $m > 2$ , and we will use this property to identify them.

We show how this is done using the  $m = 3$  spiral problem as an example (Fig. 2). In the data space [panel (a)], the items form three interlocking crescents in a spiral pattern that makes them difficult to correctly cluster by conventional means [panel (a)]. The three low-frequency clustering eigenvectors are shown in panel (b), and the representatives that we would like to find are identified by circles, triangles, and squares. To find  $\mathcal{R}_c$  we imagine that we know  $M^*$  and the corresponding assignment vectors  $\mathbf{w}_\alpha^*$  so that we can map this solution into  $\mathbb{R}^m$  at the points specified by the 3-vectors  $\bar{\mathbf{w}}^*(i) \equiv [w_1^*(i), w_2^*(i), w_3^*(i)]$  in panel (c).<sup>8</sup> Because the  $\bar{\mathbf{w}}^*(i)$  satisfy the probabilistic equality constraints, these points lie in the 2-dimensional plane that is normal to the vector  $(1, 1, 1)$  and at distance  $1/\sqrt{3}$  from the origin.

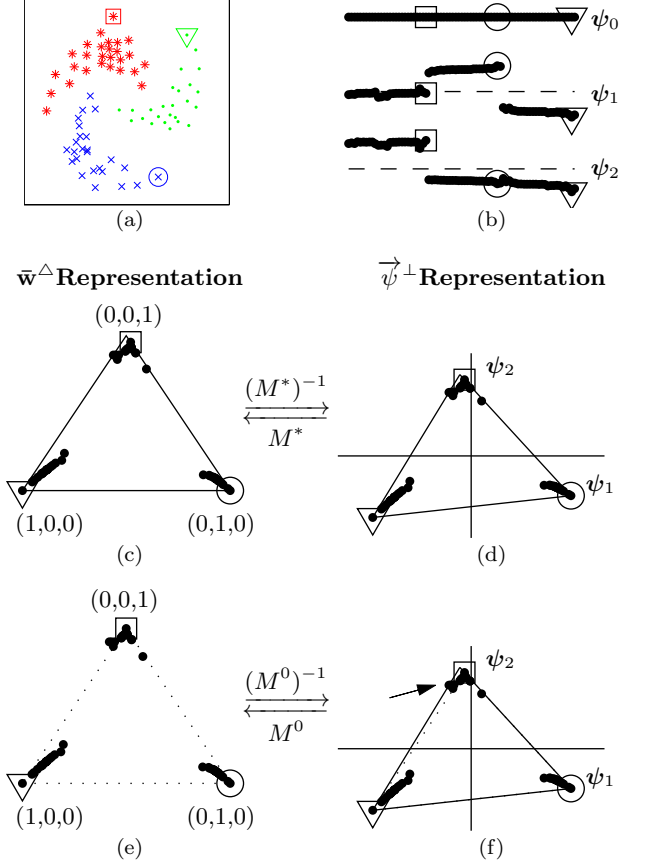


FIG. 2: (Color online)  $\bar{\mathbf{w}}^\Delta$  and  $\vec{\psi}^\perp$ -representations of the spiral problem. The items are represented by points in the 2-dimensional data-space representation (a), the clustering (low-frequency) eigenvector representation (b), the barycentric coordinates of the  $\bar{\mathbf{w}}^\Delta$ -representation (c) and (e), or the  $\vec{\psi}^\perp$ -representation (d) and (f). Panels (c) and (d) correspond to the refined solution  $M^*$ , while (e) and (f) correspond to the zeroth-order solution  $M^0$ . The solid and dotted triangles denote the  $M^*$  and  $M^0$  feasible region boundaries. [The solid triangle is superimposed in panel (f) to show how the triangle expands slightly in the  $\vec{\psi}^\perp$ -representation during refinement. The arrow indicates the item that becomes an active constraint in  $M^*$ .] The left and right arrows connecting the representations are reminders that  $M$  determines the positions of the items in the  $\bar{\mathbf{w}}^\Delta$ -representation and of the triangle vertices in the  $\vec{\psi}^\perp$ -representation. [Although it is not evident in the figure, the points in panels (c) and (e) and the top vertex in panels (d) and (f) are at slightly different positions.] The different item symbols (and colors) used in panel (a) denote the hard clustering obtained by quantizing the MDC fuzzy clustering. The ordering of items in panel (b) was chosen *post facto* to separate the clusters. The dashed lines in this panel are at  $\psi_n = 0$ . The representatives for clusters 1, 2, or 3 are enclosed within triangles, circles, or squares, respectively.

<sup>8</sup> Although they are constructed from the same components, do not confuse the  $m$   $N$ -vectors  $\mathbf{w}_\alpha^*$ , which are vectors over the space of items, with the  $N$   $m$ -vectors  $\bar{\mathbf{w}}^*(i)$ , which are vectors over the space of clusters. These vectors are the rows and columns, respectively, of the matrix  $W^*$ .

Moreover, because they satisfy the probabilistic inequality constraints, the points lie within an equilateral triangle in this plane (we use “within” to include points that lie on the boundary). This provides barycentric coordinates [27] in which the three vertices of the triangle correspond to the cluster assignments  $(1, 0, 0)$ ,  $(0, 1, 0)$  and  $(0, 0, 1)$ ; we will call these the  $\alpha = 1, 2$ , and  $3$  vertices, respectively. The three components of  $\bar{w}^*(i)$  are given by the three distances of point  $i$  from the three sides of the triangle. Thus, if point  $i$  lies on the side of the triangle opposing vertex  $\alpha$ , the inequality constraint  $w_\alpha(i) \geq 0$  is active. We call this the  $\bar{w}^\Delta$ -representation [panel (c)]. Although it is not evident in the figure, consistent with the even distribution of active inequality constraints between the clusters (Appendix B 1) each side of the triangle intersects exactly two items.

The candidate representatives are the items that are close to the three vertices, and we want to choose one each from the group near each vertex to compose  $\mathcal{R}_c$ . We can do this by choosing the three items that (when taken as vertices) define the triangle of largest area. The triangular area defined by a subset  $\mathcal{R}$  of any three items located at their solution positions is  $\det W^{*\mathcal{R}} / (2\sqrt{3})$ . Thus, our task is to identify the  $\mathcal{R}$  that maximizes the determinant.

Since we don’t actually know  $M^*$  or the  $\bar{w}^*(i)$ , how to proceed is not obvious. However, Eq. (19) implies that

$$|W^{*\mathcal{R}}| = |M^*| |\Psi^{\mathcal{R}}|,$$

so, since  $M^*$  is fixed, selecting the  $\mathcal{R}$  that maximizes  $|W^{*\mathcal{R}}|$  is equivalent to selecting the  $\mathcal{R}$  that maximizes  $|\Psi^{\mathcal{R}}|$ .

This is straightforward because  $\Psi^{\mathcal{R}}$  does not depend on  $M$ . Formally, maximizing  $|\Psi^{\mathcal{R}}|$  is a combinatoric problem that could be solved by comparing the determinants for all subsets  $\mathcal{R}$ . However, this would be exponentially expensive in  $N$ . Instead we use an efficient greedy algorithm that may not exactly maximize the determinant, but will still select the representatives solely from the subset of candidate representatives, which will be adequate to determine  $M^0$ .

We leave the details of the greedy algorithm to Appendix C, but it is useful to establish its geometric framework here while continuing to use the spiral problem as an example: We first plot each item in the 2-dimensional  $\bar{\psi}^\perp$ -representation using the 2-vector  $\bar{\psi}^\perp(i) = [\psi_1(i), \psi_2(i)]$  [panels (c) and (d)]. [No information is lost in this projection from the low-frequency subspace since  $\psi_0(i) = 1$  ( $\forall i$ ).] These vectors are independent of  $M$ ; in this representation  $M$  determines the position of the inequality constraint bounding triangle. As explained in Appendix B 4, the  $\bar{\psi}^\perp$  coordinates of the three bounding triangle vertices are the columns of the bottom two rows of  $M^{-1}$ . When  $M = M^*$  [panel (d)] the vertices may not coincide with any items, but all the items will lie within the bounding triangle. When  $M = M^0$  [panel (f)], the triangle vertices coincide with

the representatives. In this approximation some items may violate the inequality constraints and lie outside the bounding triangle. (Four items in the upper left corner are outside the triangle in this example.) The greedy algorithm operates within the  $\bar{\psi}^\perp$ -representation to identify  $\mathcal{R}^c$ .

The approach generalizes easily to higher  $m$ : the  $\bar{w}^*(i)$  are now  $m$ -vectors; the  $\bar{w}^\Delta$ -representation is in a  $(m-1)$ -dimensional hyperplane normal to the vector  $(1, 1, \dots, 1)$  in  $\mathbb{R}^m$  and provides barycentric coordinates for the  $\bar{w}^*(i)$ ;  $\mathcal{R}_c$  is identified by choosing the subset of  $m$  items that, when located at their solution positions, are the vertices of the  $m$ -simplex of largest hypervolume; the hypervolume for any subset  $\mathcal{R}$  is proportional to  $|W^{*\mathcal{R}}|$  so we can transform the problem to that of finding the  $\mathcal{R}$  that maximizes  $|\Psi^{\mathcal{R}}|$ ; this problem is equivalent to maximizing the hypervolume of the  $\bar{\psi}^\perp$ -representation simplex having vertices at  $\bar{\psi}^\perp(i) : i \in \{\mathcal{R}\}$ . Once  $\mathcal{R}_c$  has been identified, it is used to determine  $M^0$  via Eq. (25b), and  $M^0$  is used to determine the  $w_\alpha$  via Eq. (27).

### C. Refinement

#### 1. Case when $M^0$ is the exact solution

If the  $w_\alpha^0$  satisfy all the inequality constraints, then they provide the unique solution to the uncertainty minimization problem. This is easiest to prove in the  $\bar{\psi}^\perp$ -representation. Again, consider the spiral problem (Fig. 2) as an example. As discussed above, moving  $M$  from  $M^0$  moves the sides of the  $\bar{\psi}^\perp$  triangle. Moving any side inwards would leave a representative outside the triangle, thus violating an inequality constraint. And, since (in this case) all inequality constraints are satisfied, all points are already within the triangle and moving any side outwards would result in that side contacting less than two points; i.e., one of the clusters would have less than the required (Appendix B 1)  $m - 1 = 2$  active inequality constraints. Therefore, in this case  $M^* = M^0$  must be the unique solution. As can be inferred from the discussion of Fig. 1,  $M^0$  is always the unique solution for  $m = 2$  problems.

#### 2. Linearizing $\Phi(M)$

If the  $w_\alpha^0$  violate any inequality constraints, then  $M^0$  is not a solution but can be used as the starting point for further refinement. Since it is expected to be near  $M^*$ , we can expand the objective function in its neighborhood

as

$$\begin{aligned}\Phi(M) &= -\sum_{\alpha} \log \frac{\vec{M}_{\alpha} \circ \vec{M}_{\alpha}}{\vec{M}_{\alpha} \circ \vec{\varepsilon}_0} \\ &\approx \Phi(M^0) + \sum_{\alpha} \left( \vec{M}_{\alpha} - \vec{M}_{\alpha}^0 \right) \circ \vec{\nabla}_{\alpha} \Phi(M^0)\end{aligned}\quad (28)$$

where

$$\vec{\nabla}_{\alpha} \Phi(M) \equiv \left. \frac{\delta \Phi(M')}{\delta \vec{M}'_{\alpha}} \right|_{M=M'} = -2 \frac{\vec{M}_{\alpha}}{|\vec{M}_{\alpha}|^2} + \frac{\vec{\varepsilon}_0}{\vec{M}_{\alpha} \circ \vec{\varepsilon}_0}.$$

is the gradient of  $\Phi(M)$  with respect to  $\vec{M}_{\alpha}$ . Local minimization using this linear approximation and the constraints of Eq. (8) poses a linear programming (LP) problem, which can be solved by standard methods.

A simple approach would be to: (1) using Eq. (28) and all the constraints, apply LP to find an improved, constraint-satisfying solution  $M^1$ , (2) set  $M^1 \rightarrow M^0$  and repeat this procedure until sufficient convergence is achieved. This amounts to a constrained variant of gradient-descent local minimization. However, we do not expect to encounter the slow convergence problems that sometimes plague gradient descent because both the LP solution and the true solution are at vertices of the feasible polytope.<sup>9</sup> Thus, even the first iteration will drive the solution to a vertex, and the solution will not change at the next iteration unless the vertices are very dense on the scale set by the curvature of  $\Phi(M)$ . Thus, rapid convergence is expected.

### 3. Reducing the number of constraints included in LP

The cost of standard LP solvers (e.g., simplex and interior point methods) grows rapidly [ $\gtrsim O(N_c^{1.5})$ ] with the number of constraints  $N_c$ , which may be large.<sup>10</sup> While there are  $m \times N$  inequality constraints, only  $m \times (m-1)$  of these are active at  $M^*$ . These alone need to be included in the LP problem and will guarantee that all the inequality constraints will be satisfied. Since we will often be interested in problems where  $m \sim O(10)$  and  $N \gtrsim O(10^4)$ , it would accelerate the LP solver by multiple orders-of-magnitude if the number of constraints provided to the solver were reduced to  $\sim O(m)$ .

We do not know the active constraints *a priori*, but can find them rapidly by an iterative procedure that exploits the fact that (as discussed above) at  $M^*$  exactly

$m-1$  points will lie on each of the  $m$  faces of the bounding simplex in the  $\vec{\psi}^{\perp}$ -representation. To motivate it, consider the refinement of the spiral problem (Fig. 2). The right and bottom sides of the  $M^0$  triangle [panel (f)] already intersect  $m-1=2$  points each (i.e., the representatives). However, the left side must move outwards to include the four points in the upper left region that are outside the  $M^0$  triangle; this motion must leave the side intersecting two points. Because the objective function  $\Phi(M)$  constitutes an inward “pressure” on the triangle,  $M^*$  will correspond to the situation when the smallest expansion that can accomplish this is used. In this case, the left side will pivot outwards about the lower left corner until it intersects the item identified by the arrow. Each side of the resulting  $M^*$  triangle [panel (d)] will intersect two points each, and these points will be near (but not identical with) the vertices of the  $M^0$  triangle. These six intersections identify the  $m(m-1)=6$  active constraints.

This suggests that for  $m=3$  in general, the two points intersecting a side of the triangle in  $M^*$  will be near different vertices and, subject to this restriction, will be the points that are farthest outside the  $M^0$  boundary lines. This easily generalizes to  $m>3$ : none of the  $m-1$  points intersecting a face of the bounding simplex in  $M^*$  will be near to the same simplex vertex and, of the points near a vertex, it is the one that is farthest outside a face of the  $M^0$  simplex that is most likely to intersect the corresponding face of the  $M^*$  simplex. Thus, it is sensible to initially attempt a LP solution using only the inequality constraints corresponding to these  $m(m-1)$  face-point combinations. However, this is only a heuristic argument and inequality constraints may still be violated in this constraint-restricted LP solution. If so, we iterate and keep adding the violated constraints that are identified (using the same criteria) as most likely to be active to an “included constraint” list. The procedure terminates when all the inequality constraints are satisfied. Termination is guaranteed because we only add (and never remove) inequality constraints to the included constraint list. This procedure is formalized in the following algorithm:

### 4. Refinement Algorithm

1. Initialize  $\mathcal{C}$ , the set of inequality constraints provided to the LP solver, to the empty set.
2. Perform hard clustering based on the  $M^0$  assignments: Item  $i$  is assigned to cluster (vertex)  $\alpha$  if  $w_{\alpha}^0(i) > w_{\beta}^0(i)$ , ( $\forall \beta \neq \alpha$ ). We call this subset of items  $\mathcal{S}_{\alpha}$ .
3. For each  $\mathcal{S}_{\alpha}$ , determine which item is farthest outside each of the the  $m-1$  inequality constraint-boundary simplex faces that intersect at vertex  $\alpha$ . As shown in Appendix B 5, the ordering of the item points relative to the simplex faces is the same in

<sup>9</sup> We ignore the rare, case where LP may have multiple solutions.

<sup>10</sup> Interior point methods have complexity  $O(m^3 N_c^{1.5} L / \log N_c)$ , where  $L = \Omega(\log(N_c))$  [? ]. Simplex methods require  $O(\min(N_c^2, m^4))$  pivot steps [? ]. The complexity of each pivot step is  $O(N_c^2)$ , as that is the size of matrix that is updated. Thus, the number of operations for simplex methods, like that of interior point methods, scales at least as quickly as  $N_c^{1.5}$ .



the  $\bar{w}^\Delta$ - and  $\vec{\psi}^\perp$ -representations. Therefore, we determine the ordering in the barycentric coordinates of the  $\bar{w}^\Delta$ -representation since this is simple:  $w_\alpha(i)$  is the distance of an item point  $i$  from the simplex face opposite to vertex  $\alpha$  (positive if inside, negative if outside the simplex). This identifies  $m(m-1)$  inequality constraints.

4. Add whichever of these  $m(m-1)$  constraints to  $\mathcal{C}$  that are not already included.
5. Apply the LP solver with the equality constraints, the inequality constraints in  $\mathcal{C}$ , and the linear objective function approximation of Eq. (28).
6. Check for satisfaction of all inequality constraints and for convergence according to  $\max_{\alpha,i} |\mathbf{w}_\alpha^1(i) - \mathbf{w}_\alpha^0(i)| < \rho_{\text{LP}}$ , where  $\rho_{\text{LP}}$  is a small number and  $\mathbf{w}_\alpha^1(i)$  and  $\mathbf{w}_\alpha^0(i)$  are the values determined by  $M^1$  and  $M^0$ , respectively. If both conditions are satisfied terminate with  $M^* = M^1$ ; if not, set  $M^1 \rightarrow M^0$  and return to step 2.

When the algorithm is applied to the spiral problem,  $\mathcal{C}$  is set to the active constraints in a single step.<sup>11</sup>

#### D. Recursion

MDC identifies clusters based on the overall size scale of the original dataset. However, once a cluster has been identified and is considered in isolation the scale will be smaller and subclusters may be apparent. MDC can be reapplied recursively to identify such subclusters.

### IV. OVERALL COMPUTATIONAL ALGORITHM

Combining the steps described in Secs. II and III, the overall algorithm is

1. Compute and precondition  $\Gamma$  as described in Sec. II and Appendix A.
2. Compute 20 low-frequency clustering eigenvalues and eigenvectors using the iterative Lanczos

method [28? ].<sup>12</sup> The Lanczos method is usually more efficient than computation of the full eigensystem, but it will converge slowly if the eigenvalues are densely-packed near zero (as the often are). To avoid this problem we employ a shift-and-invert spectral transformation [28]

$$(\Gamma - \sigma I)^{-1} \psi_n = \nu_n \psi_n,$$

that spreads out the small eigenvalues near  $\sigma$  by transforming them into the large magnitude eigenvalues of  $(\Gamma - \sigma I)^{-1}$ ,

$$\nu_n = (\gamma_n - \sigma)^{-1}. \quad (29)$$

The eigenvectors are unaffected by the transformation, and the  $\gamma_n$  are easily calculated from Eq. (29). Since we are interested in the eigenvalues near zero, we choose  $\sigma = \sqrt{\epsilon}$ , where  $\epsilon$  is machine precision, to maximize the spread without introducing significant numerical error.

3. The lowest spectral gap satisfying Eq. (15) determines  $m$ . If there is no gap, the algorithm has determined that there are no clusters and terminates.
4. Identify the representatives and compute the zeroth-order solution  $M^0$  and  $\mathbf{w}_\alpha^0$  using the procedure of Sec. IIIB.
5. If  $\mathbf{w}_\alpha^0$  satisfies all inequality constraints,  $\mathbf{w}_\alpha^* = \mathbf{w}_\alpha^0$  and stop. Otherwise, refine  $M^0$  to  $M^*$  using the procedure of Sec. IIIC and, via Eq. (7), determine the refined solution,  $\mathbf{w}_\alpha^*$ .
6. Test the solution against the minimum certainty conditions of Eq. (16). If it satisfies them, the solution is accepted. If not, they eigenspectrum can be tested for higher spectral gaps can be tested. If desired, the fuzzy solution can be quantized to a hard clustering by assigning item each  $i$  to the cluster having the largest assignment value.
7. If desired, accepted solutions can be recursively tested for the existence of subclusters within hard clusters using the same method.

### V. RESULTS

Korenblum and Shalloway evaluated MDC by solving problems that had challenged traditional clustering methods (e.g.,  $k$ -means and agglomerative clustering) and by clustering items embedded in a 20-dimensional

<sup>11</sup> In the spiral problem the representatives at vertices 1 and 2 each contribute two active constraints. Because the left side pivots out during refinement, the representative at vertex 3 only contributes one active constraint; the second constraint associated with this vertex comes from the item identified by the arrow in Fig. 2(f). Specifically, the active constraints are  $w_\alpha(i) \geq 0$  where  $(\alpha, i) = (2, r_1), (3, r_1), (1, r_2), (3, r_2), (1, r_3)$ , and  $(2, x_3)$ , where  $x_3$  is the index of the item identified by the arrow. These are all identified by the algorithm in the first step.

<sup>12</sup> This number is somewhat arbitrary, and is chosen on the assumption that the number of potential clusters to be identified at a single level of recursion is  $< 20$ , while limiting computational cost. A larger value could be used if needed.

space to demonstrate that this success was not an artifact of low dataspace dimensionality. To extend these accuracy tests, we considered data sets from the Fundamental Clustering Problems Suite (FCPS) [29]. To test the efficiency of the new algorithm, we tested it on synthetic data sets containing up to  $N = 20,000$  items.

### A. Implementation

The C++ implementation of this algorithm was compiled using `gcc` version 4.1.2 and `g77` version 3.3.5 under `-O3` optimization. The implementation accesses low-level LAPACK [30] routines through LAPACK++ [31] version 2.5.2, interfaces to the ARPACK [32] Lanczos solver through the ARPACK++ [33] C++ wrappers, and solves constrained linear programs using the GLPK simplex method [34] version 4.9. The scaling benchmarks of Sec. V C were executed on a dedicated quad CPU 3.46 GHz Pentium 4 node, configured with 4 GB of RAM and 4 GB of swap space, and running a 64-bit version of SuSE Linux. The numerical precision parameter was  $\epsilon = 2.22045 \times 10^{-16}$ . Following Korenblum and Shalloway [8], the dataspace metric tensor  $g$  in Eq. (2) was set to the identity and the minimum gap and minimum certainty parameters were set to  $\rho_\gamma = 3$  and  $\rho_\Upsilon = 0.68$ . The LP convergence parameter was  $\rho_{LP} = 0.001$ .

### B. Performance on FCPS test sets

We tested MDC on the ten FCPS [29] data sets, which can not be clustered by  $k$ -means or agglomerative methods. Results for five of these are shown in Fig. 3 and Table I. Results for the others are not shown to conserve space, but reproduce the subjective clusterings suggested by Ultsch [29].

The Lsun [panel(a)] and Target [panel (b)] data sets contain well-separated clusters, which generate nearly disconnected  $\Gamma$ 's. If the preconditioning step (Appendix A) were not applied, the resulting numerically-degenerate systems would have multiple near-zero (incorrectly computed) eigenvalues and associated eigenvectors that would be erroneously mixed [this is the reason that the  $\psi_0$  vectors shown displayed in panels (a) and (b) are not constants.] The use of this defective eigensystem was avoided by the connected component analysis of the preconditioning step. This separated the clusters and directly determined the hard assignment vectors shown in the figures.

The  $\Gamma$  matrix of the Two Diamonds data set [panel(c)] was not disconnected, even after preconditioning. The spectral gap separating  $\gamma_1$  and  $\gamma_2$  ( $\gamma_2/\gamma_1 = 29.3$ ) properly indicated that there are  $m = 2$  clusters. MDC computed the fuzzy assignment vectors shown in the figure. As discussed above,  $m = 2$  problems are trivial for MDC, so the  $M^0$  solution was exact and no LP iterations were required. Appropriately, the assignments were very strong

(1.00) for items in the middle of the diamonds and weak ( $\sim 0.5$ ) for items near their interface, reflecting the expectation that these items should not be strongly assigned to either cluster. For the most part, the weakly-assigned items are the ones that we have found to be misclassified by single- and complete-linkage methods and  $k$ -means (not shown). The overall certainties  $\bar{\Upsilon}_\alpha$  were high (0.93) for both clusters.

The Tetra data set [panel (d)] has four nearly-overlapping tetrahedrally-arranged clusters in a three-dimensional dataspace. MDC correctly determined  $m = 4$  from the spectral gap and produced an appropriate fuzzy clustering. As in the case of Two Diamonds, items near the cluster interfaces were given weaker cluster assignments, in this case ranging down to  $w_\alpha(i) = 0.74$ .

The Engy Time data set [panel (e)] is an overlapping two-dimensional mixture of two Gaussian distributions. The preconditioning step removed a few outliers from the dataset, but because of the strong overlap, MDC assigned all the items to a single cluster. This differs from Ultsch [29], who used a self-organizing map approach incorporating distance and density relations to divide the items into two clusters. We suggest that either choice is acceptable, depending on the application.

Problem	$m$	$\frac{\gamma_m}{\gamma_{m-1}}$	$\bar{\Upsilon}_\alpha(M)$	Assignments	LP Iterations
Lsun	4	$> \epsilon^{-1/2}$	1.00	Hard Clustering	—
Target	6	$> \epsilon^{-1/2}$	1.00	Hard Clustering	—
Two Diamonds	2	29.30	0.93	0.53–1.00	0
			0.93	0.59–1.00	
Tetra	4	17.20	0.87	0.74–1.00	2
			0.90	0.77–1.00	
			0.91	0.87–1.00	
			0.93	0.55–1.00	
Engy Time	1	—	—	—	—

TABLE I: Quantitative analysis of MDC on bi- and tri-variate Fundamental Clustering Problems Suite test cases. The number of clusters  $m$ , the magnitude of the spectral gap  $\gamma_m/\gamma_{m-1}$ , the cluster certainties  $\bar{\Upsilon}_\alpha(M)$ , the range of assignment values for each cluster, and the number of iterations of the linear programming solver are listed for each problem.  $\gamma_m/\gamma_{m-1} > \epsilon^{-1/2}$ , where  $\epsilon$  is numerical precision, signals that the clusterings were determined by the connected component analysis during the preconditioning phase.

### C. Computational efficiency and scaling

To systematically evaluate MDC efficiency and cost scaling with  $N$ , we applied it to synthetic data sets containing from 2 to 10 clusters and from 5,000–20,000 items arranged in a pyramid in a two-dimensional data space. These problems required from two to four invocations of the LP solver, with the number increasing with  $m$ , but not evidently with  $N$ . The log-log plot in Fig. 4 shows that there is a clear power-law relation between

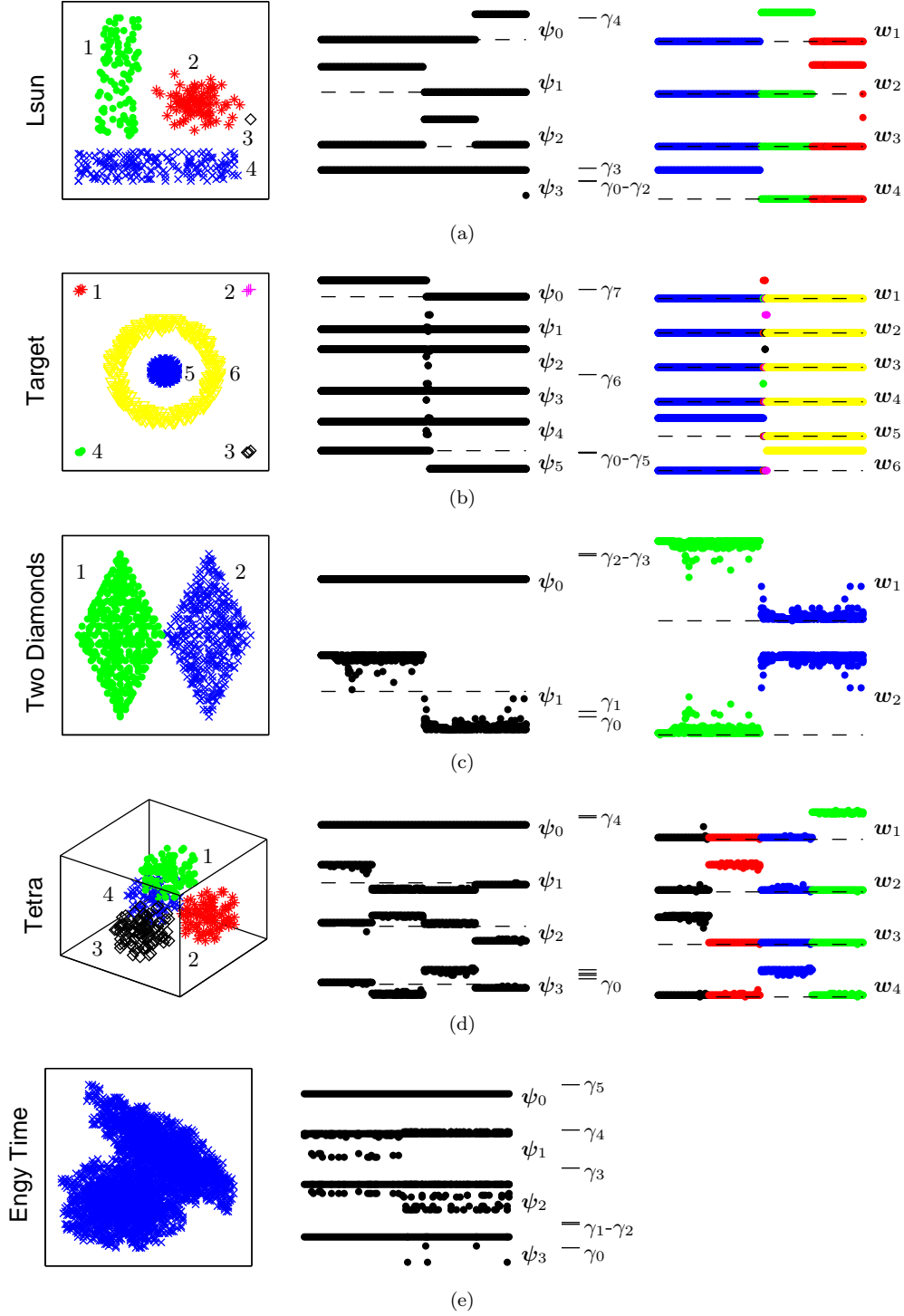


FIG. 3: (Color online) Macrostate data clustering of test cases from the Fundamental Clustering Problems Suite. The (a) Lsun, (b) Target, (c) Two Diamonds, (d) Tetra, and (e) Engy Time problems are shown. The data set (left column), eigenvectors  $\psi_n$  and eigenvalues  $\gamma_n$  (middle column), and assignment vectors  $w_\alpha$  (right column) are shown. The different item symbols (and colors) in the left column denote the hard clustering obtained by quantizing the MDC fuzzy clustering; the numbers correspond to the cluster identifiers used in the right column. The ordering of items in the middle and right columns was chosen *post facto* to separate the clusters and would not be evident before the cluster analysis. The points in these panels do not overlap, but only appear to because of limited graphical resolution. The eigenfunctions in Lsun and Target are those output by the numerical eigensolver. Because of numerical error they are incorrectly mixed and  $\psi_0$  is not a constant. They are shown for illustration only; as discussed in the text, the solution in this case is determined by the connected component analysis of the preconditioning step.

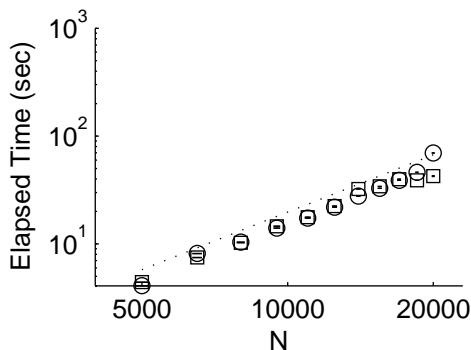


FIG. 4: Log-log plot of elapsed wall clock time versus  $N$  for synthetic benchmarks.  $N$  is varied from 5,000 to 20,000 in steps of 1,500. The results shown for  $m = 2$  (○) and  $m = 10$  (□) are representative of those for intermediate  $m$ . They are averages over five runs. (the standard errors of the mean are too small to be discernible.) The dotted line is the least-squares linear fit and has slope 1.7.

$N$  and execution time: the average slope over all problems indicates a computational scaling of  $O(N^{1.9})$ , with little dependence on  $m$ . Execution time was dominated (typically  $\sim 99\%$ ) by the time required to compute the sparse  $\Gamma$  matrix. The time required for the largest problem ( $m = 10$ ,  $N = 2 \times 10^4$ ) was only about one minute using a commodity personal computer. Such problems are of the scale of biological microarray gene expression data sets. The scaling suggests that it may be possible to handle problems with  $N$  as large as  $\sim O(10^6)$  with overnight runs on serial machines. Execution time was dominated by the calculation of Gamma and by the eigensolver (each having roughly equal cost), with other contributions totaling less than 4

## VI. DISCUSSION

Macrostate data clustering (MDC) is a fuzzy  $m$ -way spectral clustering method that is motivated by an analogy to the coarse-graining of a physical diffusive system. The method uses a heuristic approximation to the physical transition rate matrix as the Laplacian matrix  $\Gamma$  for spectral clustering. By exploiting non-linear information preserved in the eigensystem of  $\Gamma$  MDC succeeds on problem types where traditional methods such as  $k$ -means and agglomerative clustering fail. Its  $m$  low-lying eigenvectors serve as a linear basis for the expansion of the assignment vectors  $\mathbf{w}_\alpha$ , which probabilistically describe cluster membership. The inherent fuzziness of the  $\mathbf{w}_\alpha$  introduces cluster overlap and attendant uncertainty, which leads naturally to an information-theoretic objective function based on the principle of uncertainty minimization. Uncertainty minimization determines the expansion coefficients of the linear combination. Further,

a minimum macrostate certainty condition, along with a spectral gap condition, directly determines the number of clusters  $m$ . Here we have described an efficient, two-phased approach to solving the non-convex minimum uncertainty optimization problem that performs non-linear refinement of a zeroth-order solution through a series of local, linear optimizations. The zeroth-order solution is a heuristic approximation to simplex volume maximization in the space spanned by the  $m$  low-lying eigenvectors, which is itself an approximation to uncertainty minimization.

This heuristic was previously used within PCCA [20] for the same purpose as our own: to select representatives and assign their respective membership function values to induce a clustering over the full item space. However, its use within PCCA is motivated from the perspective of matrix perturbation theory of block-diagonal  $\Gamma$  matrices [21]. PCCA is derived from work [35, 36] exploiting the near-level eigenvector structure induced by small perturbations, which in turn lead to small fluctuations in the level structure of the resulting assignment vectors, as shown in Fig. 5(a). In particular, Weber [37] proves that the zeroth-order solution defining  $m$  clusters is feasible whenever the convex hull of all  $N$  items is an  $m - 1$ -simplex, as when  $\Gamma$  is block diagonal and hence represents completely disconnected clusters or *invariant subsets*. In this case,  $\Gamma$  has an  $m$ -fold degenerate ground state with corresponding eigenvectors of level structure. The eigenvector level structure and, hence, the simplex structure, are perturbed only to second order by an  $O(\epsilon)$  perturbation to the block-diagonal  $\Gamma$  [20, 38]. Therefore, the approach is applicable whenever there are small-scale deformations to the eigenvectors. In contrast, the minimum uncertainty objective of MDC motivates, and is approximated by, volume maximization. As volume maximization is itself approximated by the zeroth-order solution, PCCA clustering, induced by that solution, approximates the minimum uncertainty solution, which is ultimately derived by our refinement step. The volume maximization condition is less restrictive than a perturbation condition: it requires only that at least one item (i.e., the representative) be well assigned to each cluster. Thus, the zeroth-order approximation is more generally applicable than previously believed; it suffices even for data sets whose clusters are not crisply defined, but instead are described by overlapping (or uncertain) assignment vectors, as in Fig. 5(b).

The minimum uncertainty objective function quantifies a quality clustering. It thus enables MDC to iteratively explore a region of the  $m^2$ -dimensional solution space through local optimization. Searching in the vicinity of a solution is particularly relevant to methods such as PCCA, which are justified by a perturbation analysis of invariant sets. In such cases, the solution determined may be “best” for the unperturbed system, but merely within the neighborhood of a better solution to the perturbed system.



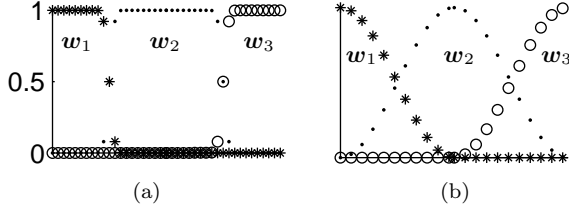


FIG. 5: (a) Nearly level assignment vector (and hence eigen-vector) structure away from macrostate boundaries is not required for a zeroth-order solution. (b) Instead, the weaker condition that one item from each cluster be nearly perfected assigned suffices for its validity.

Deuffhard and Weber [38] similarly use an objective function, as well as explicit probabilistic constraints, to cluster protein conformations collected from molecular dynamics simulations. The zeroth-order solution over a reduced set of unconstrained variables defines an initial point from which to initiate a local, Nelder-Mead optimization of the non-convex objective function. The complete set of variables are then defined by substituting the unconstrained variables into constraint equations. This procedure is iterated until convergence of the objective function, which may be selected either to maximize the metastability of a symmetric Markov matrix derived from molecular dynamics trajectories or to maximize the *scaling* of the membership functions (i.e., to force a cluster's maximum assignment towards unity). Metastability may be expressed as

$$\sum_{\alpha} \frac{\langle \mathbf{w}_{\alpha} | e^{-\Gamma t} | \mathbf{w}_{\alpha} \rangle}{\langle \mathbf{1} | \mathbf{w}_{\alpha} \rangle},$$

where the transition rate matrix  $\Gamma$  acts as the generator of the Markov matrix  $e^{-\Gamma t}$ . Thus, the uncertainty objective function may be viewed as the first-order approximation of this metastability. In fact, the latter reduces to the former as  $t$  approaches zero. As clustering results are presumably dependent on the choice of  $t$ , its selection should be justified. In practice [39, 40],  $t$  is set to a multiple of the molecular dynamics integration time step used to generate trajectories (e.g., 40-50 fs). The scaling objective function

$$\sum_{\alpha} \max_i w_{\alpha}(i) \leq m.$$

is also related to the uncertainty objective function. Maximizing the former forces at least one assignment per cluster close to unity and, given the equality constraints, tends to minimize uncertainty. However, it does not account for cluster size. Therefore, forcing the maximum assignment of a small cluster close to unity at the expense of a larger cluster will not affect scaling, though it will properly result in greater uncertainty.

The view that data items are sampled from a continuous, but unknown, probability distribution and that they

evolve according to a diffusive model has significant consequences. It is the lack of an equivalent dynamical interpretation that prevent [20] the authors of PCCA from applying the above metastability condition to data clustering. Further, the Smoluchowski equation influences the form of the  $\Gamma$  matrix by demanding, from dimensional analysis, that it have units of inverse distance squared and by fixing the exponential scale factor through consideration of probability interception.

This relation between clustering and diffusion has as its origin the statistical coarse-graining of physical systems [18, 41]. Hence, such methods are readily applied to the study of protein dynamics, where  $\Gamma$  is directly defined from molecular dynamics trajectories [38, 39, 40, 42, 43] and the items are configurations or microstates sampled by the simulation. Once the macrostates are defined, a series of short trajectories may be initiated from each to determine long-time kinetic properties [42]. Alternately, configuration space may be coarse-grained through consideration of the equilibrium probability  $p_B$  [18]. This approach also provides dynamical system properties, but without the need for simulation within either the fine- or coarse-grained configuration space. Under either strategy, the coarse-grained system describes transitions between the physically-relevant states and thus provides a practical alternative to long, fine-grained simulations for deriving properties such as state lifetimes [44] and mean first-passage times [45]. Fuzzy spectral clustering addresses the particular requirements of detecting macrostates: its flexibility in determining cluster shape accommodates the basins in high-dimensional configuration space that are unlikely to be strictly convex, while its weak, fuzzy assignment of some configurations motivates their characterization as “transition states” [37]. Applying the solution proposed here to a matrix  $\Gamma$  derived from simulation data would allow comparison of the uncertainty minimization objective function with the metastability objective function of PCCA, previously applied in this context [39].

Other important biological domains would similarly benefit from the fuzziness and flexible cluster shapes of MDC. As in the aforementioned population genetics [2, 3], fuzzy assignments allow overlapping of communities in complex networks, with high cluster certainty instead indicating a community's robustness [46]. Indeed, spectral methods have recently been used to analyze network structure and dynamics [47]. Fuzzy approaches are also relevant to the clustering of gene expression data: gene functional redundancy and the multiple roles of proteins are likely to result in overlapping gene clusters, which can not be represented by the hard clusters of traditional methods [48].

Aside from expressing overlap, fuzziness implies uncertainty: low assignment probabilities indicate that the corresponding items deserve special consideration, while those assigned with high probability may be quickly verified or trusted outright. An ability to efficiently determine items likely to be incorrectly classified would ben-

efit manually-curated databases, such as the structural classification of proteins (SCOP) database [49]. Using structural and evolutionary information, domain experts locate a protein domain within the SCOP hierarchy describing, from least to most constraining, its class, fold, superfamily, and family. Domains within the same superfamily are believed to be related evolutionarily. Though the manual curation process [50] is aided by automatic methods, there remains a significant lag time separating the addition of a structure to the PDB [51] and its classification within SCOP: As of May 13, 2008, the PDB contained 50,830 entries, while the most recent distribution of SCOP in Nov, 2007 contained only 34,494 PDB entries. SCOP distributions occur at most every several months and, often, much less frequently. Fuzzy clustering may be able to alleviate the lengthy curation process. Paccanaro et al. [52] have already shown that a spectral clustering method can faithfully reproduce many of the superfamily classifications from a subset of SCOP. MDC provides the additional benefit of indicating the confidence of a particular classification. Thus, misclassifications should be reflected by relatively low assignment probabilities, which would signal, either to a curator or to a researcher attempting to extend SCOP with a new structure, that a structure deserves manual consideration.

Biological data sets pose special difficulties for clustering methods: they are noisy and likely contain obfuscating irrelevant dimensions. For example, only a subset of genes will have expression levels correlated with the experimental condition of interest (e.g., cancer). Further, the subset of relevant genes may vary across experimental conditions. Indeed, in a study of a mRNA [53], items were found to cluster on a small and varying fraction of their measurement dimensions. To accommodate such data, COSA [53] assigns non-uniform relevance to each dimension by manipulating the metric tensor  $g$  of Eq. (2). It does so through an iterative search that invokes a clustering procedure at each step. As such, it could be incorporated with MDC.

We anticipate that MDC will be less sensitive to irrelevant dimensions than traditional methods since the diffusional model asserts that items are most significantly affected by their nearest neighbors. Irrelevant dimensions are those that do not distinguish a cluster or alternately are those that have large intra-cluster dispersion. Due to the exponential scaling factor cutoff  $\langle d_0^2 \rangle$ , intra-cluster, nearest-neighbor distances make a near constant contribution to the transition rate. Therefore, the intra-cluster transition between items is linearly related to the number of intervening items. However, items within different clusters have significant separation along some relevant dimension, which leads to an exponential decrease in their transition rate. Hence, irrelevant dimensions contribute a linear, entropic effect, whereas relevant dimensions give rise to an exponential, energetic effect. The result is analogous to a system governed by the Arrhenius equation, wherein the transition rate between states is described by an entropic prefactor that multiplies a fac-

tor exponential in the energetic difference between the states. As MDC is less sensitive to irrelevant dimensions than traditional methods, it should more quickly converge under the iterative COSA framework.

## VII. ACKNOWLEDGMENTS

Support was provided by a DOE High-Performance Computer Science Fellowship administered by The Krell Institute, Ames, IA. We are grateful to Sally McKee for the use of computational resources and to Vince Weaver for help in administering them.

## APPENDIX A: $\Gamma$ PRECONDITIONING

Numerical errors can obscure the differences between very small eigenvalues and obfuscate the spectral gap when the range between  $\gamma_1$  and  $\gamma_{N-1}$  is too large to be faithfully represented numerically. This can occur if clusters are nearly isolated (and hence communicate very slowly) or when two items within a cluster are exceedingly close to another (and hence communicate very rapidly). The former case also occurs when the problem contains outliers—items that are distant from the bulk of the items. We avoid this problem by preconditioning  $\Gamma$ . In addition, we improve computational efficiency by sparsifying  $\Gamma$  by setting very small transition rates exactly to zero and employing efficient sparse matrix algorithms.

To avoid the numerical error problems, we want to precondition  $\Gamma$  so that

$$\gamma_1 \gg \Delta_\gamma, \quad (\text{A1})$$

where  $\Delta_\gamma$  is the expected computational error in the eigenvalues. Typically [30, 32]

$$\Delta_\gamma \leq \epsilon \gamma_{N-1},$$

where  $\epsilon$  is machine precision. To conservatively satisfy Eq. (A1), we want to adjust the very small and/or very large elements of  $\Gamma$  so that

$$\left( \frac{\gamma_1}{\gamma_{N-1}} \right)^2 \gtrsim \epsilon. \quad (\text{A2})$$

To minimize the effect of this adjustment on the other eigenvalues, this adjustment should yield a  $\gamma_1$  and  $\gamma_{N-1}$  that are multiplicatively symmetric relative to  $\gamma_{\text{mid}}$ , an appropriate midrange frequency. That is, we require

$$\frac{\gamma_{\text{mid}}}{\gamma_1} \sim \frac{\gamma_{N-1}}{\gamma_{\text{mid}}}. \quad (\text{A3})$$

Eqs. (A2) and (A3) will be satisfied if

$$\gamma_1 \gtrsim \gamma_{\text{mid}} \epsilon^{1/4} \quad (\text{A4a})$$

$$\gamma_{N-1} \lesssim \gamma_{\text{mid}} \epsilon^{-1/4}. \quad (\text{A4b})$$

To determine  $\gamma_{\text{mid}}$ , we note that  $-\Gamma_{i>}$ , the magnitude of the largest off-diagonal element in row  $i$  of  $\Gamma$ , determines the largest transition rate connecting  $i$  to other items. Thus, the median of the  $-\Gamma_{i>}$  is a reasonable choice for  $\gamma_{\text{mid}}$ . However, to maximize the useful numerical range, if it appears that one, but not the other, of the inequalities in Eq. (A4a) are likely to be satisfied without any adjustment, then we shift  $\gamma_{\text{mid}}$  to take advantage of this. Specifically,

$$\begin{aligned} &\text{If } (\min |\Gamma_{ij}| < \gamma_{\text{mid}} \epsilon^{1/4}) \cap (\max |\Gamma_{ij}| < \gamma_{\text{mid}} \epsilon^{-1/4}) \\ &\quad \text{then } \gamma_{\text{mid}} \rightarrow \max |\Gamma_{ij}| \epsilon^{1/4} \\ &\text{If } (\min |\Gamma_{ij}| > \gamma_{\text{mid}} \epsilon^{1/4}) \cap (\max |\Gamma_{ij}| > \gamma_{\text{mid}} \epsilon^{-1/4}) \\ &\quad \text{then } \gamma_{\text{mid}} \rightarrow \min |\Gamma_{ij}| \epsilon^{-1/4}, \end{aligned}$$

where  $|\Gamma_{ij}|$  refers to the magnitudes of the off-diagonal elements.

### 1. Connected component analysis

To satisfy Eq. (A4a) we perform a standard connected component analysis [54] using threshold

$$\gamma_{\text{lo}} = \gamma_{\text{mid}} \epsilon^{1/4}. \quad (\text{A5})$$

This analysis initially assigns items to individual sets and then iteratively merges sets whenever any of their respective members have connecting connectivities  $|\Gamma_{ij}| > \gamma_{\text{lo}}$ . If distinct sets (i.e., disconnected components) remain at the end, then the algorithm creates hard assignment vectors identifying them. In some cases the disconnected components may be outliers. However, in other cases they will be significant clusters that, if desired, can be recursively subjected to another round of analysis to check for subclusters.

### 2. High transition rate cutoff

We expect that  $\gamma_{N-1}$  will be of the order of the fastest inter-item transition rate in the system.<sup>13</sup> Thus, we can satisfy Eq. (A4b) by truncating any off-diagonal elements of  $\Gamma$  exceeding

$$\gamma_{\text{hi}} \equiv \gamma_{\text{mid}} \epsilon^{-1/4};$$

i.e.,  $\Gamma_{ij} \rightarrow -\min(|\Gamma_{ij}|, \gamma_{\text{hi}})$ .

<sup>13</sup> Inter-item transition rates can combine to generate eigenvalues that are higher than the individual rates. But, since we expect that each item will communicate rapidly only with a relatively small number of near neighbors (even for large  $N$ ), we don't expect  $\gamma_{N-1}$  to exceed  $\max |\Gamma_{ij}|$  by a factor that is significant on the scale of  $\epsilon^{-1/4}$ , so this effect be ignored.

## 3. Sparsification

To reduce memory requirements and improve cache performance, we represent  $\Gamma$  as a sparse matrix by setting very small elements (i.e.,  $|\Gamma_{ij}| < \gamma_{\text{lo}}/10$ ) to zero. This improves eigensolver efficiency so that MDC may be practically applied to large problems. For example, for the largest of the scaling benchmarks considered in Section V.B. (i.e.,  $m = 10$ ,  $N = 20,000$ ), the sparse  $\Gamma$  matrix held less than 870,000 elements and thus reduced storage by a factor of nearly 500.

<sup>14</sup>

## 4. Diagonal elements

Once the steps above, which modify only the off-diagonal elements of  $\Gamma$ , have been completed, we reset the diagonal elements according to Eq. (10b) so that Eq. (4b) is again satisfied.

## APPENDIX B: VARIOUS PROOFS

### 1. Even distribution of active inequality constraints

We prove here that each cluster must be constrained by exactly  $m-1$  inequality constraints at each local minimum of  $\Phi$  in the feasible region. Consider a local minimum in the asymmetric  $M$ -representation discussed in Sec. III A. Korenblum and Shalloway [8] have already proved that this must be at a vertex of the feasible polytope. The coordinates of the individual free particles at the local minimum,  $\vec{M}_\alpha^\times$  ( $1 \leq \alpha < m$ ), all satisfy the inequality constraints of Eq. (8a), but the homogeneity of these constraints means that they will also be satisfied for any  $\xi_\alpha \vec{M}_\alpha$  with  $\xi_\alpha > 0$ . Therefore, the active inequality constraints acting on the free particles leaves the  $m-1$  degrees-of-freedom of the  $\xi_\alpha$  ( $1 \leq \alpha < m$ ) unspecified. Thus, they are inadequate to force  $\vec{M}^{\times \text{free}}$  to be at a vertex of the feasible polytope. Therefore, at least  $m-1$  additional active constraints must come from the inhomogeneous inequality constraints Eq. (18) associated with the slave particle. However, the choice of the slave particle [i.e., in Eq. (17) is arbitrary. Therefore, *every*

<sup>14</sup> In computational practice, we sparsify  $\Gamma$  based on the values of the corresponding distances  $d_{ij}$  before the  $\Gamma_{ij}$  are computed from Eq. (10a). This saves unnecessary exponentiations for the large fraction of elements of  $\Gamma_{ij}$  that will be set to 0 anyway. For this purpose, we set  $\Gamma_{ij} \rightarrow 0$  whenever  $d_{ij} > d_{\text{max}}$ , where  $d_{\text{max}}$  is calculated by numerically inverting Eq. (10a) for  $\Gamma_{ij} \rightarrow -\gamma_{\text{lo}}/10$ . In this procedure,  $\gamma_{\text{mid}}$ , which is needed to compute  $\gamma_{\text{lo}}$ , is computed by substituting  $d_{ij} = \text{median}\{d_{i<}\}$  into Eq. (10a).

particle must have at least  $m - 1$  active inequality constraints. But since only  $m(m - 1)$  inequality constraints are active at a vertex, each of the  $m$  particles must have *exactly*  $m - 1$  inequality constraints active. It is easy to see that this proof extends to every vertex of the feasible polytope except for those vertices where at least one of the  $\vec{M}_\alpha^\times = 0$  (since multiplying this by  $\xi_\alpha$  does not move the particle). The proof does not preclude the possibility that a single item may be associated with multiple active constraints; i.e., it is possible that  $w_\alpha(i) = 0$  and  $w_\beta(i) = 0$  are both active constraints. (For example, this is the case for the solution to the spiral problem [Figs. 2(c) and (d)] where  $w_2(r_1) = 0 = w_3(r_1)$  and also  $w_1(r_2) = 0 = w_3(r_2)$ .)

## 2. Invertibility of $\Psi^\mathcal{R}$

We prove here that there is at least one subset of  $m$  items  $\mathcal{R}$  such that  $\Psi^\mathcal{R}$  is invertible. Since the  $m$  rows of  $\Psi$ , i.e., the  $m$  low-frequency eigenvectors, are linearly independent,  $\Psi$  has rank  $m$ . Therefore,  $\Psi$  also has at least  $m$  linearly-independent columns. If the items corresponding to these columns are selected to comprise  $\mathcal{R}$ , then the  $m \times m$  matrix  $\Psi^\mathcal{R}$  has full rank and is therefore invertible.

## 3. Invertibility of $M$

$M$  that satisfy the constraints of Eqs. (8) can be chosen that are not invertible. However, we prove here that each  $M$  corresponding to a local minimum of  $\Phi$  within the feasible region is invertible: As proved in Appendix B 1, at any such minimum each cluster has  $m - 1$  active inequality constraints; i.e.,  $(m - 1)$  items lie on each of the  $m$  faces of the bounding simplex in the  $\bar{w}^\Delta$ -representation. Consider a subset of  $m$  of these items,  $\mathcal{R}$ , which contains one item from each face. It defines an  $m$ -simplex (inscribed within the bounding simplex) that will have non-zero hypervolume. This hypervolume is proportional to  $|W^\mathcal{R}|$ , implying that  $|W^\mathcal{R}| \neq 0$  and, with Eq. (22), implying that  $|M| \neq 0$ . Thus,  $M$  is invertible. This proof depends only on the even distribution of active inequality constraints (and not the local minimum), so it actually extends to every vertex of the feasible polytope in the asymmetric representation where all the  $\vec{M}_\alpha \neq 0$ , since we have proven in Appendix B 1 that all the inequality constraints are evenly distributed at such vertices.

## 4. The bounding simplex in the $\vec{\psi}^\perp$ -representation

Analogously to Eq. (19), we may write

$$W^{\text{vert}} = M \circ \Psi^{\text{vert}}, \quad (\text{B1})$$

where the rows of  $\Psi^{\text{vert}}$  are the coordinates of the bounding simplex vertices in the low-frequency eigenvector representation and  $W^{\text{vert}} = I$  is the matrix whose rows are the coordinates of the vertices in the  $\bar{w}$ -representation. Inverting this gives  $\Psi^{\text{vert}} = M^{-1}$ . When  $M = M^0$  this and Eq. (25b) imply that  $\Psi^{\text{vert}} = \Psi^{\mathcal{R}_c}$ , which is consistent with the placement the zeroth-order placement of the representatives at the vertices. When  $M = M^*$ , the vertices may not correspond to item locations, but, as proved in Appendix B 3,  $M^*$  is invertible, so  $\Psi^{\text{vert}} = (M^*)^{-1}$ . In both cases, the simplex vertex coordinates in the  $\vec{\psi}^\perp$ -representation are given by the rows of  $\Psi^{\text{vert}}$  with the first component omitted. (Just as for  $\Psi^\mathcal{R}$ , all elements in the first column of  $\Psi^{\text{vert}}$  are unity for any invertible  $M$ ,<sup>15</sup> in particular, for  $M^0$  and  $M^*$ .)

## 5. Ordering of item points in the $\bar{w}^\Delta$ and $\vec{\psi}^\perp$ -representations

To simplify the discussion we use the spiral problem illustrated in Fig. 2 as a specific example. The proof is easily generalized. We will refer to the vertices by the corresponding cluster indices, which are easily read off in the  $\bar{w}^\Delta$ -representation. For example, the top vertex in panel (c), which has coordinates (0,0,1) is vertex 3. For simplicity we denote this as point  $v_3$ . We do the same for the other vertices and carry the same labeling over to the  $\vec{\psi}^\perp$ -representation.

Determining the item ordering relative to the bounding simplex faces is easy in the  $\bar{w}^\Delta$ -representation: Because these provide barycentric coordinates, the distance of a point  $i$  from the side opposite to vertex  $\alpha$  is just  $w_\alpha(i)$  with the sign negative if the point lies outside the simplex. Thus, the ordering is determined simply by comparing these distances. We relate this ordering to the ordering in the  $\vec{\psi}^\perp$ -representation in a few steps. First, note that the distance of point  $i$  from the side opposite  $v_2$  is linearly related to the area of the triangle having vertices at points  $i$ ,  $v_1$ , and  $v_3$ , with sign depending on triangle orientation. This signed area is proportional to

$$A = \frac{\det[\bar{w}(i) \otimes \hat{e}_1 \otimes \hat{e}_3]}{\det[\hat{e}_2 \otimes \hat{e}_1 \otimes \hat{e}_3]},$$

where  $\bar{w}(i) \otimes \hat{e}_1 \otimes \hat{e}_3$  is the  $3 \times 3$  matrix formed by stacking the three row vectors and the denominator (which will always be  $\pm 1$ ) is inserted so that the sign will be correct. Second, note that since

$$\begin{aligned} [\bar{w}(i) \otimes \hat{e}_1 \otimes \hat{e}_3] &= M \circ [\vec{\psi}(i) \otimes \vec{\psi}(v_2) \otimes \vec{\psi}(v_3)] \\ &\text{and} \\ [\hat{e}_2 \otimes \hat{e}_1 \otimes \hat{e}_3] &= M \circ [\vec{\psi}(v_2) \otimes \vec{\psi}(v_1) \otimes \vec{\psi}(v_3)], \end{aligned}$$

<sup>15</sup> To prove this, multiply both sides of Eq. (21) by  $M_{n\beta}^{-1}$  and sum over  $n = 0, \dots, m - 1$ . This gives  $1 = M_{0\beta}^{-1}$ .



where  $\vec{\psi}(v_k)$  is the  $m$ -vector having the coordinates of vertex  $v_k$  in the low-frequency eigenvector space, we have

$$A = \frac{\det[\vec{\psi}(i) \otimes \vec{\psi}(v_1) \otimes \vec{\psi}(v_3)]}{\det[\vec{\psi}(v_2) \otimes \vec{\psi}(v_1) \otimes \vec{\psi}(v_3)]}. \quad (\text{B2})$$

Third, since all the vectors in Eq. (B2) have  $\psi_0 = 1$ ,  $A$  is proportional to the signed area of the triangle having vertices  $i$ ,  $v_1$ , and  $v_3$  in the  $\vec{\psi}^\perp$ -representation, which will be positive if  $i$  is within the triangle and negative if it is outside the triangle. Fourth, this area is proportional to the distance of point  $i$  from the side opposite to  $v_2$ . Combining all these proportionalities proves that the distance of point  $i$  from the side opposing a vertex in the  $\vec{\psi}^\perp$ -representation is proportional to the distance in the  $\vec{\psi}^\perp$ -representation.

### APPENDIX C: GREEDY ALGORITHM FOR SELECTING $\mathcal{R}$

The goal of the algorithm is to choose the subset of items  $\mathcal{R}$  whose convex hull, which is an  $m$ -simplex, has maximum hypervolume  $V_m$  in the  $\vec{\psi}^\perp$ -representation. If one face of the simplex is already determined,  $V_m$  is proportional to the distance of the excluded vertex from that face. [For example, in the case of a 3-simplex (a triangle), this is the familiar area =  $1/2$  base  $\times$  height rule, where “base” is the hyperarea length of a specified simplex face and “height” is the distance of the other point from that face.] This suggests a natural greedy algorithm: (a) initialize by finding the  $(q = 2)$ -simplex of greatest hypervolume, (b) extend the  $q$ -simplex to and

$(q + 1)$ -simplex by finding the item that is furthest from the hypersurface that embeds the  $q$ -simplex, (c) return to step (b) until  $q = m$ .

Specifically,

#### 1. Initialize:

Select the two items  $i_1$  and  $i_2$  that maximize  $\|\vec{\psi}^\perp(i_2) - \vec{\psi}^\perp(i_1)\|$ .  
 $\mathcal{R} = \{i_1, i_2\}$ .  
 $q = 2$ .

#### 2. Stop if $q = m$ .

#### 3. Iterate:

(a) Select the item  $i_{q+1}$  that maximizes

$$d^\perp(i_{q+1}) = \|\mathcal{P}^q \circ [\vec{\psi}^\perp(i_{q+1}) - \vec{\psi}^\perp(i_1)]\|,$$

where

$$\mathcal{P}_{nn'}^q = I_{nn'} -$$

$$\sum_{q'=2}^q \frac{[\vec{\psi}(i_{q'}) - \vec{\psi}(i_1)]_n [\vec{\psi}(i_{q'}) - \vec{\psi}(i_1)]_{n'}}{\|[\vec{\psi}(i_{q'}) - \vec{\psi}(i_1)]\|^2}.$$

(b)  $\mathcal{R} \rightarrow \mathcal{R} \cup i_{q+1}$

(c)  $q \rightarrow q + 1$

(d) Return to step 2.

Here  $\circ$  denotes the inner product within the  $(m - 1)$ -dimensional  $\vec{\psi}^\perp$  space and  $\mathcal{P}^q$  is the projection matrix in this space that removes the components of  $[\vec{\psi}^\perp(i_{q+1}) - \vec{\psi}^\perp(i_1)]$  that lie within the subspace containing the  $q$ -simplex. Therefore,  $d^\perp(i_{q+1})$  is the distance of  $\vec{\psi}^\perp(i_{q+1})$  from the subspace, and the  $(q + 1)$ -simplex formed by adding  $\vec{\psi}(i_{q+1})$  as a vertex is the  $(q + 1)$ -simplex of maximum hypervolume that contains the previously computed  $q$ -simplex as one of its faces.

- 
- [1] R. J. Cho, M. J. Campbell, E. A. Winzler, L. Steinmetz, A. Conway, L. Wodicka, T. G. Wolfsberg, A. E. Gabrielian, D. Landsman, D. J. Lockhart, et al., *Molecular Cell* **2**, 65 (1998).
  - [2] J. K. Pritchard, M. Stephens, and P. Donnelly, *Genetics* **155**, 945 (2000).
  - [3] N. Patterson, A. L. Price, and D. Reich, *PLoS Genet.* **2**, 2074 (2006).
  - [4] B. S. Everitt, S. Landau, and M. Leese, *Cluster Analysis* (Arnold, London, 2001).
  - [5] J. Shi and J. Malik, in *Proceedings of IEEE Conference on Computer Vision and Pattern Recognition* (1997), pp. 731–737.
  - [6] S. D. Kamvar, D. Klein, and C. D. Manning, in *Proc. International Joint Conference on Artificial Intelligence* (2003).
  - [7] A. Y. Ng, M. I. Jordan, and Y. Weiss, in *Proceedings of the 14th Neural Information Processing Systems Conference* (2002).
  - [8] D. Korenblum and D. Shalloway, *Phys. Rev. E* **67**, 056704 (2003).
  - [9] C. J. Alpert, A. B. Kahng, and S.-Z. Yao, *Discrete Applied Mathematics* **90**, 3 (1999).
  - [10] D. A. Spielman and S.-H. Teng, in *Proc. Annual Symposium on Foundations of Computer Science* (IEEE Computer Society, Washington, DC, 1996), pp. 96–105.
  - [11] S. T. Barnard and H. D. Simon, *Concurrency: Practice and Experience* **6**, 101 (1994).
  - [12] P. K. Chan, M. D. F. Schlag, and J. Y. Zien, in *ACM IEEE Design Automation Conference* (ACM Press, New York, NY, 1993), pp. 749–754.
  - [13] H. D. Simon and S.-H. Teng, *SIAM J. Scientific Computing* **18**, 1436 (1997).
  - [14] D. Verma and M. Meilă, Tech. Rep. UW CSE 03-05-01, University of Washington (2003).
  - [15] M. Meilă and J. Shi, in *Proc. International Workshop on Artificial Intelligence and Statistics* (2001).
  - [16] L. Zelnik-Manor and P. Perona, in *Proc. Neural Information Processing Systems Conference* (2004).
  - [17] H. S. Chan and K. A. Dill, *Phys. Today* **46**, 24 (1993).
  - [18] D. Shalloway, *J. Chem. Phys.* **105**, 9986 (1996).
  - [19] M. B. Eisen, P. T. Spellman, P. O. Brown, and D. Botstein, *Proc. Natl. Acad. Sci. USA* **95**, 14863 (1998).
  - [20] M. Weber, W. Rungtaritvotin, and A. Schliep, Tech.

- Rep. 04-39, Konrad-Zuse-Zentrum für Informationstechnik Berlin (2004).
- [21] G. W. Stewart, in *Mathematical Computer Performance and Reliability*, edited by G. Iazeolla, P. J. Courtois, and A. Hordijk (Elsevier, North Holland, 1984), pp. 287–302.
  - [22] M. Belkin and P. Niyogi, *Neural Computation* **15**, 1373 (2003).
  - [23] D. Harel and Y. Koren, in *Proc. Conference on Foundations of Software Technology and Theoretical Computer Science* (Springer-Verlag, London, UK, 2001), pp. 18–41.
  - [24] B. Nadler, S. Lafon, R. R. Coifman, and I. G. Kevrekidis, *Applied and Computational Harmonic Analysis* **21**, 113 (2006).
  - [25] L. Yen, D. Vanvyve, F. Wouters, F. Fouss, M. Verleyesen, and M. Saerens, in *Proc. European Symposium on Artificial Neural Networks* (2005), pp. 317–324.
  - [26] G. L. Scott and H. C. Longuet-Higgins, in *Proceedings of British Machine Vision Conference* (1990), pp. 103–108.
  - [27] H. S. M. Coxeter, *Introduction to Geometry* (John Wiley & Sons, 1969), 2nd ed.
  - [28] R. Lehoucq and D. Sorensen, in *Templates for the Solution of Algebraic Eigenvalue Problems: A Practical Guide*, edited by Z. Bai, J. Demmel, J. Dongarra, A. Ruhe, and H. van der Vorst (SIAM, Philadelphia, 2000).
  - [29] A. Ultsch, in *Workshop on Self-Organizing Maps* (Paris, 2005), pp. 75–82.
  - [30] E. Anderson, Z. Bai, S. Blackford, J. Demmel, J. Dongarra, J. Du Croz, A. Greenbaum, S. Hammarling, A. McKenney, and D. Sorensen, *LAPACK Users' Guide* (SIAM, Philadelphia, PA, 1999).
  - [31] C. Stimming, *Lapack++* <http://lapackpp.sourceforge.net> (2008).
  - [32] R. B. Lehoucq, D. C. Sorensen, and C. Yang, *ARPACK Users' Guide: Solution of Large-Scale Eigenvalue Problems with Implicitly Restarted Arnoldi Methods* (SIAM, Philadelphia, 1998).
  - [33] F. A. M. Gomes and D. C. Sorensen, Tech. Rep. TR97729, Rice University (1997).
  - [34] A. Makhorin, *GNU linear programming kit: Reference manual* <http://www.gnu.org/software/glpk> (2006).
  - [35] P. Deuffhard, W. Huisinga, A. Fischer, and C. Schütte, *Lin. Alg. Appl.* **315**, 39 (2000).
  - [36] C. Schütte and W. Huisinga, *Handbook of Numerical Analysis* **X**, 699 (2003).
  - [37] M. Weber and T. Galliat, Tech. Rep. 02-12, Konrad-Zuse-Zentrum für Informationstechnik Berlin (2002).
  - [38] P. Deuffhard and M. Weber, *Lin. Alg. Appl.* **398**, 161 (2005).
  - [39] S. Kube and M. Weber, *J. Chem. Phys.* **126**, 024103 (2007).
  - [40] F. Noé, I. Horenko, C. Schütte, and J. Smith, *J. Chem. Phys.* **126**, 155102 (2007).
  - [41] C. Schütte, A. Fischer, W. Huisinga, and P. Deuffhard, *J. Comput. Phys.* **151**, 146 (1999).
  - [42] J. D. Chodera, W. C. Swope, J. W. Pitera, and K. A. Dill, *Multiscale Model. Simul.* **5**, 1214 (2006).
  - [43] J. D. Chodera, N. Singhal, V. S. Pande, K. A. Dill, and W. C. Swope, *J. Chem. Phys.* **126**, 155101 (2007).
  - [44] W. C. Swope, J. W. Pitera, and F. Suits, *J. Phys. Chem. B* **108**, 6571 (2004).
  - [45] N. Singhal, C. D. Snow, and V. S. Pande, *J. Chem. Phys.* **121**, 415 (2004).
  - [46] J. Reichardt and S. Bornholdt, *Phys. Rev. Lett.* **93**, 218701 (2004).
  - [47] P. N. McGraw and M. Menzinger, *Phys. Rev. E* **77**, 031102 (2008).
  - [48] A. P. Gasch and M. B. Eisen, *Genome Biology* **3**, 1 (2002).
  - [49] A. G. Murzin, S. E. Brenner, T. Hubbard, and C. Chothia, *J. Mol. Biol.* **247**, 536 (1995).
  - [50] S. E. Brenner, C. Chothia, T. J. P. Hubbard, and A. G. Murzin, *Methods in Enzymology* **266**, 635 (1996).
  - [51] H. M. Berman, J. Westbrook, Z. Feng, G. Gilliland, T. N. Bhat, H. Weissig, I. N. Shindyalov, and P. E. Bourne, *Nucleic Acids Research* **28**, 235 (2000).
  - [52] A. Paccanaro, J. A. Casbon, and M. A. S. Saqi, *Nucl. Acids Res.* **34**, 1571 (2006).
  - [53] J. H. Friedman and J. J. Meulman, *J. R. Statist. Soc. B* **66**, 1 (2004).
  - [54] T. H. Cormen, C. E. Leiserson, R. L. Rivest, and C. Stein, *Introduction to Algorithms* (MIT Press, Cambridge, MA, 2001), chap. 22.3.